5D INTERPOLATION AND REGULARIZATION WITH WAVEFRONT ATTRIBUTES

Y. Xie and D. Gajewski

email: *yujiang.xie@studium.uni-hamburg.de*
keywords: *5D interpolation, wavefront attributes, differential evolution (DE)*

ABSTRACT

RTM and FWI usually require regularly spaced data. However, as some natural and anthropogenic reasons, real 3D seismic data, sometimes, are irregularly and sparsely sampled, which will restrict the usage of the RTM and FWI in actual applications. As an interpolation technique to regularize and enhance the quality of data with low signal-to-noise (S/N), the partial 3D common-reflection-surface (CRS) method was proposed. However, two potential problems still need to be addressed while extending this technique into a 5D interpolation and regularization. The fundamental one is that the CRS wavefront attributes would be better determined simultaneously by a global search strategy. The second one is that an azimuth-based regularization would be considered in different azimuth direction, which will benefit for a further anisotropic traveltime operator. With the 3D SEG/EAGE C3WA data as an example, our results indicated that the partial 3D CRS can perform well in the 5D interpolation and regularization if the above two problems are addressed.

INTRODUCTION

3D prestack data are generally recorded in 5D data space. As some natural and anthropogenic factors, the 3D prestack data are often irregularly and sparsely sampled during data acquisition, which would affect the quality of many wave-equation migration and inversion methods, such as reverse time migration (RTM) (e.g., Baysal et al., 1983), full wavefield inversion (FWI) (see e.g., Virieux and Operto, 2009). In order to resolve this problem, one simply method is to introduce an interpolation approach. As a traveltime-based interpolation technique to regularize and enhance the quality of data with low signal-to-noise (S/N), the partial common-reflection-surface (CRS) method was proposed by Baykulov and Gajewski (2009), which can use geological information from neighboring CMP gathers, thus significantly increase the S/N after the interpolation. In the 3D case, the partial 3D CRS (Baykulov and Gajewski, 2010) was proposed. It is actually a 5D interpolation technique in the time domain. However, two potential problems are still needed to be resolved in this technique. The fundamental one is that the CRS wavefront attributes would be better determined by a global search strategy. The second one is that, in each 3D CMP gather, an azimuth-based regularization will be considered. The azimuth-based regularization will benefit for an anisotropic traveltime operator. In order to perform a global CRS search, the differential evolution (DE) algorithm (Storn and Price, 1997) is applied. As examples, the 3D SEG/EAGE C3WA data are applied.

THEORY

The partial 3D CRS traveltime operator can be derived from the classical hyperbolic 3D CRS traveltime approximation (e.g., Müller, 2003):

$$t_{hyp}^2 = (t_0 + \mathbf{w}_z^T \mathbf{m}_d)^2 + \mathbf{m}_d^T \mathbf{N} \mathbf{m}_d + \mathbf{h}^T \mathbf{M} \mathbf{h}, \tag{1}$$

where $\mathbf{w}_z$ includes the near-surface velocity (v_0), the dip (α) and azimuth (λ) of the reference ray. The midpoint parameter satisfies: $\mathbf{m}_d = \mathbf{m} - \mathbf{m}_0$, where $\mathbf{m}_0$ is a considered CMP position, and $\mathbf{m}$ is a neighboring midpoint of the considered CMP. Parameter $\mathbf{h}$ is half offset. The 2×2 symmetrical matrices $\mathbf{M}$ and $\mathbf{N}$ are related to the curvatures of the normal-incidence-point (NIP) wavefront and the normal (N) wavefront, respectively. The superscript T denotes the transpose of a matrix.

To constructe the partial 3D CRS operator, the ZO traveltime $t_{0,p}$ of the partial 3D CRS operator is required. For one sample A on an arbitrary trace with half offset $\mathbf{h}$ = (*offx*, *offy*), the $t_{0,p}$ can be found or fitted by

$$t_{22}^2(offx, offy) = t_{11}^2 + \mathbf{h}^T\mathbf{M}\mathbf{h}. \tag{2}$$

We assume the ZO traveltime $t_{0,p} = t_{11}$ if the calculated t_{22} satisfies: $(t - t_{22})^2 \leq fmin^2$, where t_{11} is the trial ZO traveltime along the ZO trace, and t_{22} is the hyperbolic traveltime calculated by Equation 2. The coefficient $fmin$ can be automatically computed by the wavefront attributes of two neighboring ZO samples around the fitted $t_{0,p}$. A refinement of the $t_{0,p}$ with sample A is unnecessary if the ZO attributes obtained from $t_{0,p}$ is worse or if the wavefront attributes at $t_{0,p}$ have a strong local variation. The wavefront attributes at $t_{0,p}$ can be read from the attribute files after the $t_{0,p}$ is determined. Hence we construct the partial 3D CRS opeator by

$$t_{hyp,p}^2 = (t_{0,p} + \mathbf{w}_z^T\mathbf{m}_d)^2 + \mathbf{m}_d^T\mathbf{N}\mathbf{m}_d + \mathbf{h}^T\mathbf{M}\mathbf{h}. \tag{3}$$

Equation 3 is a 5D interpolation operator in the 5D data space: one temporal dimension and four spatial dimensions. With the 5D interpolation operator, one can interpolate a simple at A ($m_{0,x}$, $m_{0,y}$, $offx$, $offy$, t), where $\mathbf{m}_d$ = ($m_{0,x}$, $m_{0,y}$).

METHOD

Differential Evolution

We perform a global CRS wavefront attribute search with the DE algorithm, which is a variant of evolutionary algorithms solved an optimization problem by the evolutionary ideas of natural selection. The DE algorithm has been used in many fields and has already shown good convergence properties (Price et al., 2006). The general DE mutation operator is given by

$$N_{i,j} = P_{r1,j} + F(P_{r2,j} - P_{r3,j}), \tag{4}$$

where $r1$, $r2$ and $r3$ are three random agents picked from the generation. They must be distinct from each other as well as distinct from the considered agent. Generally, the differential weight F is set between [0 2]. For each agent i, the mutant operator is

$$[U_{i,j} = \begin{cases} N_{i,j} & p_j < CR \; or \; j = L, \\ P_{i,j} & Otherwise. \end{cases}] \tag{5}$$

where CR is the crossover probability set between [0 1], $p_j \in$ [0 1], and L is an integer randomly generated between [0 7]. In this work, the parameters F and CR are estimated from the data. Alternatively, a good choice of the F and CR for various optimization problems was suggested by Pedersen (2010). The accuracy of the wavefront attributes generated by the DE algorithm is checked by the semblance (e.g., Neidell and Taner, 1971). In each generation, the agents are updated with a higher semblance and the set of wavefront attributes with the best semblance is kept for the next generation.

Azimuth-based regularization

Azimuth-based regularization can be considered in a 3D CMP gather. The trace location to be regularized in each considered CMP gather is given by $\mathbf{h}$ = ($offx$, $offy$). For each azimuth direction $iaz * \delta\lambda$ in the CMP gather, seeing Figure 1, we have $offy = tan(0 + iaz * \delta\lambda) * offx$, where $\delta\lambda$ is azimuth interval, and iaz indicates different azimuth direction. The $offx$ is given by $offx = k * \delta h_x$, where δh_x is the half-offset increment in the x direction, and integer $k = 0, 1, 2, ..., intmax(h_x)/\delta h_x$. The intmax() retures

the integer part of the maximum h_x. With the relationship of $offx$ and $offy$, a full, wide or narrow azimuth regularization within [0 2π] can be chosen freely in the considered 3D CMP gather (see Figure 1). The $\delta\lambda$ and δh_x should be predetermined by users in different data. With the 3D SEG/EAGE C3WA data as an example, the azimuth range regularized here only set between [π/4, π/2] in each 3D CMP gather (see Figure 1c), where we use $\delta\lambda = 15 * \pi/180$ and δh_x = 40 m. The streamer-line direction is referenced as azimuth = π/2 since the 3D SEG/EAGE C3WA data has long offset in h_y direction.

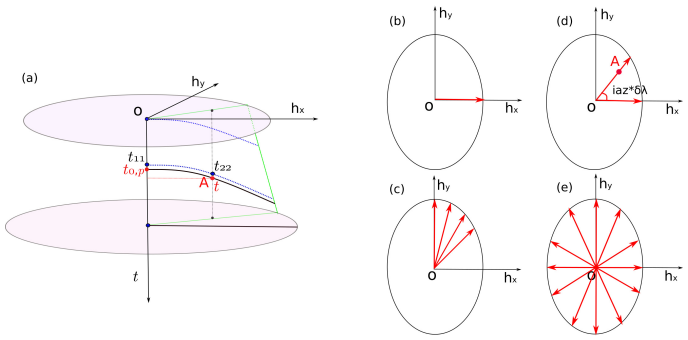

Figure 1: Determination of $t_{0,p}$ with a traveltime fitting operator (a) and different azimuth regularization strategies. (b) Fixed azimuth regularization (e.g., azimuth = 0). (c) Narrow azimuth regularization. (d) Regularizing a trace at position $A(offx, offy)$ with azimuth of $iaz * \delta\lambda$. (e) Wide- or full-azimuth regularization.

EXAMPLES AND RESULTS

Examples shown in this work use the 3D SEG/EAGE C3WA open data. Figure 2a shows its velocity model. More details about the SEG/EAGE salt data can be found in the SEG Wiki open data. A preprocessing for the SEG/EAGE data is shown by Xu et al. (2004). To demonstrate the performance of the CRS-based interpolation method, some traces in the data are randomly killed and a random Gaussian noise with S/N = 10 was added to the seismograms. Figure 2b show a CMP gather (CDP 182113) with gaps. For the sake of simplicity, in this CMP gather, only traces with a fixed azimuth = π/2 are shown. We can see that the S/N of the gather is increased significantly after the interpolation. The conclusions from other azimuths are the same and not shown here, e.g., azimuth = $5\pi/12$, $\pi/3$, $\pi/4$, all of which illustrate that a high-quality data can be achieved if the partial 3D CRS is applied with the globally determined wavefront attributes.

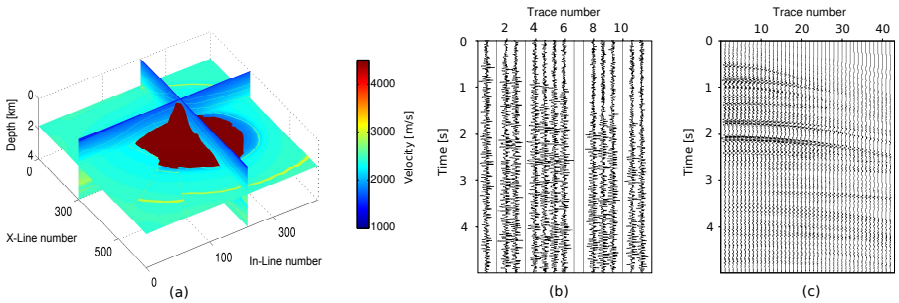

Figure 2: Velocity of the 3D SEG/EAGE model (a) (Xie and Gajewski, 2016), and one CMP gather before (b) and after (c) the partial 3D CRS method, where the CRS wavefront attributes are determined globally with the DE algorithm.

To better reveal the salt body after the interpolation, two common-offset sections of the interpolation volume are shown. Figure 3 shows inline 220 of the first common-offset volume, i.e., **h** = (0, 0). Figure 4 illustrates inline 220 of the second common-offset volume, i.e., **h** = (0, 1000). Both the zero- and far-offset inline sections indicate that the data quality is improved after the partial 3D CRS method, especially un-

der the salt body and the large gap area (Figure 4a), where the gaps are filled with information from its neighboring traces of current CMP and its neighboring CMPs. The wavefront attributes used here are determined from the DE algorithm. The interpolation results with wavefront attributes from the conventional pragmatic approach are not shown here due to their poor image quality, which will be given in our other work.

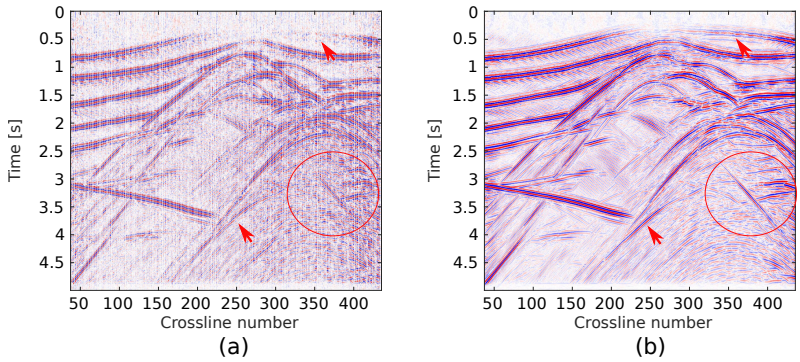

Figure 3: Inline 220 of zero offset volume. (a) Raw gapped section. (b) Section with partial 3D CRS method. Here all traces have the same half offset **h** = (0, 100), and each CMP has only one trace.

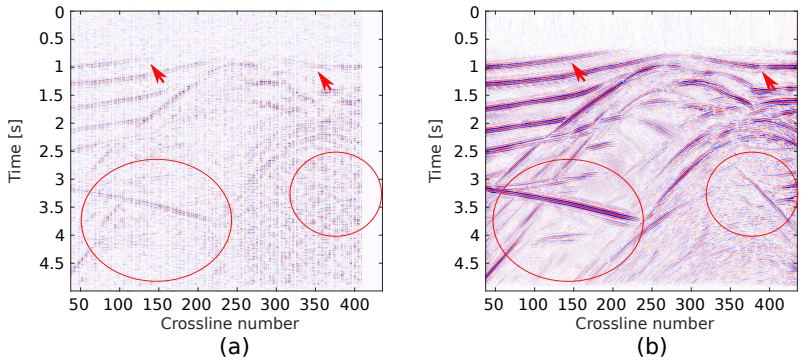

Figure 4: Inline 220 of a far common-offset volume. (a) Raw gapped section, particularly see the right side gap. (b) Section with partial 3D CRS method. Here all traces have the same half offset **h** = (0, 1000), and each CMP has only one trace.

CONCLUSIONS

We extend the partial 3D CRS method into a 5D interpolation and regularization technique, where the CRS wavefront attributes would be better determined by a global search strategy, e.g., the evolutionary-based DE algorithm. An azimuth-based regularization within each 3D CMP gather is also presented here. Selection of different azimuth regularization strategies in the CMP gather is data dependent. Limited by the offset range of the 3D SEG/EAGE C3WA data, only the classical hyperbolic 3D CRS method is shown in this work. For a data with very large offsets, the 3D non-hyperbolic CRS or 3D finite-offset CRS could be applied straightforward, and the anisotropic traveltime operators can also be utilized if the data input has anisotropic properties.

ACKNOWLEDGEMENTS

We thank the Applied Seismics Group Hamburg for continuing discussion and thank the sponsors of WIT Consortium and SEG for providing the data. Y. Xie appreciates the support through the China CSC for funding parts of this work.

REFERENCES

Baykulov, M. and Gajewski, D. (2009). Prestack seismic data enhancement with partial common-reflection-surface (CRS) stack. *Geophysics*, 74:V49–V58.

Baykulov, M. and Gajewski, D. (2010). Partial 3D CRS Stack. In *72nd EAGE Conference and Exhibition incorporating SPE EUROPEC 2010*.

Baysal, E., Kosloff, D., and Sherwood, J. (1983). Reverse time migration. *Geophysics*, 48:1514–1524.

Müller, N. (2003). The 3D Common-Reflection-Surface Stack - Theory and Application. In *Diploma thesis, University of Karlsruhe*.

Neidell, N. and Taner, M. (1971). Semblance and other coherency measures for multichannel data. *Geophysics*, 36:482–497.

Pedersen, M. (2010). Good Parameters for Differential Evolution. In *Hvass Laboratories Technical Report HL1002*.

Price, K., Storn, R., and Lampinen, J. (2006). Differential evolution: a practical approach to global optimization. In *Springer Science & Business Media*.

Storn, R. and Price, K. (1997). Differential evolution - a simple and efficient heuristic for global optimization over continuous spaces. *Journal of Global Optimization*, 11:341–359.

Virieux, J. and Operto, S. (2009). An overview of full-waveform inversion in exploration geophysics. *Geophysics*, 74:WCC1–WCC26.

Xie, Y. and Gajewski, D. (2016). Simultaneous estimation of the 3D CRS attributes by an evolutionary-based Nelder-Mead algorithm. In *SEG Technical Program Expanded Abstracts 2016*, pages 4326–4330.

Xu, S., Lambare, G., and Calandra, H. (2004). Fast migration/inversion with multivalued ray fields: Part 2 - Applications to the 3D SEG/EAGE salt model. *Geophysics*, 69:1320–1328.